

## Three novel isograds in metamorphosed siliceous dolomites from the Ballachulish aureole, Scotland

JOHN M. FERRY

Department of Earth and Planetary Sciences, Johns Hopkins University, Baltimore, Maryland 21218, U.S.A.

### ABSTRACT

Isograds were mapped in siliceous dolomites from the Ballachulish aureole on the basis of the formation of geikielite ( $\text{MgTiO}_3$ ), baddeleyite ( $\text{ZrO}_2$ ), and qandilite ( $\text{Mg}_2\text{TiO}_4$ ) by the following model reactions: rutile + dolomite = geikielite + calcite +  $\text{CO}_2$ , zircon + 2 dolomite = baddeleyite + forsterite + 2 calcite + 2  $\text{CO}_2$ , and geikielite + periclase = qandilite. The ( $T$ ,  $X_{\text{CO}_2}$ ) conditions of reaction inferred from (1) mineral equilibria in pelitic rocks, (2) calcite + dolomite thermometry, and (3) the diopside + dolomite + forsterite + calcite + tremolite and dolomite + periclase + calcite equilibria are: geikielite isograd (640–655 °C, 0.76–0.80); baddeleyite isograd (660–710 °C, 0.76–0.95); qandilite isograd (725–755 °C, <0.08). These  $T$ - $X_{\text{CO}_2}$  conditions for the geikielite and baddeleyite isograds are the same within error of those independently estimated from rutile + dolomite + geikielite + calcite and zircon + dolomite + baddeleyite + forsterite + calcite equilibria using Berman's thermodynamic data base. Rutile, zircon, geikielite, and baddeleyite are common in dolomites from at least two other contact aureoles in Scotland and Montana. Although the minerals occur in concentrations <0.01%, they appear to have been in local equilibrium during metamorphism both with each other and with coexisting carbonates and silicates and are potentially useful but currently unexploited records of the physical conditions of metamorphism.

### INTRODUCTION

Siliceous dolomitic limestones continue to play a key role in petrologists' efforts to understand mineral reactions and chemical processes during metamorphism at least since the classic study of Bowen (1940). Bowen recognized that progressive metamorphism under most conditions resulted in a sequence of now well-known reactions that could be mapped in the field as tremolite, forsterite, diopside, periclase, and wollastonite isograds. The other members of Bowen's sequence, monticellite, akermanite, spurrite, merwinite, and larnite, develop less commonly during especially high-temperature or low-pressure metamorphism. Tilley (1948) later argued that talc forms prior to tremolite in some cases. This study documents that there exists an additional, complementary sequence of prograde mineral reactions in metamorphosed siliceous dolomites involving trace minerals that occur in concentrations <0.01%, including geikielite, baddeleyite, and qandilite. Although the report describes development of these minerals in the Ballachulish contact aureole, Scotland, ongoing work in several other aureoles indicates that these minerals are more likely not recognized than rare. Mineral equilibria involving geikielite, baddeleyite, rutile, zircon, forsterite, and carbonates provide useful, unappreciated constraints on temperature and fluid composition during contact metamorphism of siliceous dolomites.

### GEOLOGIC SETTING

The Ballachulish igneous complex and its contact metamorphic aureole was recently the subject of a comprehensive, interdisciplinary investigation (Voll et al. 1991). The plutonic rocks are composed of monzodiorite, quartz diorite, and granite. The plutonic rocks intrude Dalradian metasedimentary units that include the Appin Phyllite, Ballachulish Slate, and Leven Schist. Siliceous limestones and dolomites are interbedded with the Appin Phyllite and Ballachulish Slate and form mappable units, the Appin and Ballachulish Limestones. The sedimentary rocks were first recrystallized at ~6 kbar and ~500 °C during Dalradian regional metamorphism at 490–520 Ma and then contact metamorphosed at  $412 \pm 28$  Ma by the Ballachulish igneous complex. With increasing grade of contact metamorphism, isograds were mapped in pelitic rocks on the basis of the appearance of (1) cordierite + biotite, (2) cordierite + potassium feldspar or andalusite + biotite + quartz (in different bulk compositions), (3) andalusite + potassium feldspar, (4) corundum + potassium feldspar, and (5) silicate melt (Pattison and Harte 1991). Pressure during contact metamorphism was ~3 kbar and maximum temperatures were ~750 °C (Pattison 1991).

This study focuses on contact metamorphosed siliceous dolomites mapped as Appin Limestone in the Allt Guibhsachain area located in the northeast corner of the

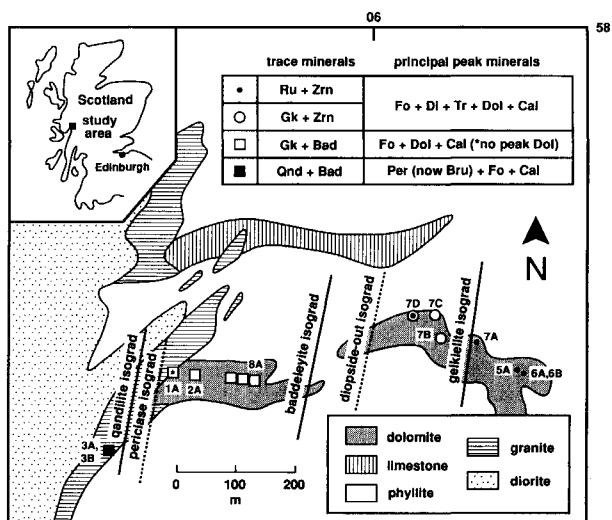


**FIGURE 1.** Geologic sketch map of the Allt Guibhsachain area in the northeast corner of the Ballachulish aureole, Scotland (from Weiss 1986 and Masch and Heuss-Aßbichler 1991). Symbols are sample localities; numbers inside border refer to samples described in text and tables; numbers outside border refer to the National Grid Reference System. Gk = geikielite, Bad = baddeleyite, Qnd = qandilite; other mineral abbreviations follow Kretz (1983). Isograds labeled on high-grade side. Diopside (Di)-out and periclase (Per) isograds from Ferry (unpublished manuscript).

aureole (Fig. 1). Masch and Heuss-Aßbichler (1991) identified isograds based on the formation of forsterite and periclase in the dolomites, presented some mineral chemical data, proposed prograde mineral reactions involving calcite, dolomite, forsterite, tremolite, diopside, and periclase, and estimated peak  $PTX_{CO_2}$  conditions of contact metamorphism. Heuss-Aßbichler and Masch (1991) described mineral textures in the metacarbonate rocks and speculated on mineral-fluid reaction mechanisms.

#### METHODS OF INVESTIGATION

As part of a broader study of fluid flow during contact metamorphism 14 samples of siliceous dolomite were collected at 12 locations in the Allt Guibhsachain area (Fig. 1). Mineral assemblages were identified by optical and scanning electron microscopy. Qualitative analyses of all minerals were obtained by EDS with the JEOL JXA-8600 electron microprobe at Johns Hopkins University. Minerals that exhibited detectable deviation from ideal compositions were analyzed quantitatively with WDS with the use of natural silicate and carbonate mineral standards and a ZAF correction scheme (Armstrong 1988). Modes of the 14 samples were measured by counting at least 2000 points in thin section with back-scattered electron imaging. Any uncertainty in the identification of a particular point was resolved by obtaining an EDS X-ray spectrum.

**TABLE 1.** Modes of selected samples of metamorphosed siliceous dolomites

Sample	1A	2A	3A	3B	7A	7C	8A
Calcite	61.05	21.08	46.09	50.51	19.77	48.97	10.91
Dolomite	6.00	59.95	18.71	17.06	46.82	8.25	78.82
Forsterite	16.65	2.70	0.25	0.53	4.03	3.49	0.79
Diopside	0	0	0	0	2.14	2.65	0
Brucite (Per)*	0	0	9.60	11.20	0	0	0
Brucite (Srp)*	0.55	0.05	2.46	1.70	0	0	0.05
Mica**	1.20	2.80	0	0	6.41	4.32	tr
Spinel	0.75	0.05	0.44	0.39	0	0	0.29
Tremolite	0.25	1.62	0	0	9.13	1.62	tr
Chlorite	0	0.34	0	0	0.10	0.05	0.29
Serpentine	13.30	11.40	22.45	18.61	11.61	30.26	8.80
Apatite	0	0	0	0	tr	0.10	0.05
Pyrrhotite	0.25	tr	0	tr	0	0.29	0
Sphalerite	0	tr	0	0	0	0	0
Zircon	0	0	0	0	tr	tr	0
Rutile	0	0	0	0	tr	0	0
Geikielite	tr	tr	0	0	0	tr	tr
Baddeleyite	tr	tr	tr	tr	0	0	tr
Qandilite	0	0	tr	tr	0	0	0

Note: Values given in volume percent; tr = <0.05%. Sample numbers refer to Figure 1. Numbers in normal type identify exclusively prograde minerals; numbers in italics identify exclusively retrograde minerals; underlined numbers identify minerals that formed during both prograde and retrograde metamorphism in the same sample.

\* (Per), after periclase; (Srp), intergrown with serpentine after forsterite.  
\*\* Mica in sample 1A is kinoshitalite; mica in all other samples is phlogopite.

#### MINERALOGY AND MINERAL CHEMISTRY

##### Principal minerals

Modes of seven representative siliceous dolomites are listed in Table 1. Compositions of peak and some retrograde minerals appear in Table 2. The 14 samples can be divided into three groups based on their principal peak minerals. Rocks 400–500 m from the contact contain forsterite + diopside + tremolite + dolomite + calcite + phlogopite (open and solid circles, Fig. 1). Assemblages in samples collected from this interval differ somewhat from those reported by Masch and Heuss-Aßbichler (1991) and are the subject of another report (Ferry, unpublished manuscript). Minerals observed in samples collected closer to the pluton are the same as reported by Masch and Heuss-Aßbichler (1991). Dolomites 0–200 m from the contact contain forsterite + dolomite + calcite + mica + spinel (open squares, Fig. 1). Location 3 is one of several dolomite xenoliths in granite that contained periclase + forsterite + calcite + spinel at the peak of metamorphism (solid square, Fig. 1).

All siliceous dolomites contain an abundance of retrograde minerals (see footnote to Table 1). Peak periclase has been hydrated to brucite. Dolomite in samples from locations 1 and 3 is retrograde, and retrograde dolomite occurs with peak dolomite in the other samples. Serpentine is the most abundant silicate mineral in all but one sample (1A) and makes up >30% of some rocks (e.g., 7C). Secondary chlorite was produced by retrograde reaction of spinel with forsterite and calcite. Secondary tremolite in samples <200 m from the contact is the product of retrograde alteration of forsterite (e.g., samples

1A, 2A, 8A, Tables 1 and 2). More detailed documentation of the retrograde minerals and a model that quantitatively interrelates temperature, fluid composition, fluid flow, and reaction progress during their formation are presented by Ferry (unpublished manuscript).

The compositions of dolomite, forsterite, diopside, and spinel are close to Mg-rich Fe-Mg solutions with  $Fe/(Fe + Mg) \leq 0.07$  (Table 2). Calcite compositions fall in two groups. Although both groups are practically Ca-Mg solutions, the most magnesian calcite inclusions in forsterite are typically much more Mg-rich than matrix calcite. Calcite inclusions were analyzed for Si to verify that their more magnesian compositions are not an artifact of contamination by host olivine. The most magnesian calcite inclusions in forsterite are believed to preserve peak compositions or nearly so; compositions of matrix calcite have been partially reset during cooling by exsolution of dolomite. Of the principal peak minerals tremolite deviates most from an ideal composition (e.g., samples 7A and 7C), largely by the edenite ( $NaAlSi_{-1}$ ) and tschermakite ( $Al_2Mg_{-1}Si_{-1}$ ) substitutions. Retrograde tremolite is nearly an Fe-Mg solution with  $Fe/(Fe + Mg) \leq 0.03$  (samples 1A, 2A, and 8A). Mica in most samples is too altered for meaningful determination of composition; a limited number of analyses indicate that with the exception of sample 1A mica is close to ideal phlogopite with  $Fe/(Fe + Mg) \leq 0.02$ . Micas have Cl contents below detection by EDS. Values of  $F/(F + OH)$  are low ( $<0.03$ ) in analyzed micas within 200 m of the contact;  $F/(F + OH) = 0.09-0.10$  in micas from locations 5 and 6. Mica in sample 1A, located  $\sim 2$  m from the contact between granite and dolomite, is the unusual barium potassium mica kinoshitalite. Because no Ba-bearing mineral was observed in dolomites at lower grades, the formation of kinoshitalite probably involved metasomatic transfer of Ba from the adjacent pluton.

#### Trace minerals

In addition to the principal peak and retrograde minerals, the metamorphosed siliceous dolomites contain a suite of trace minerals that occur in concentrations  $<0.3\%$  by volume, including apatite, pyrrhotite, sphalerite, zircon, rutile, geikielite, baddeleyite, and qandilite (Table 1). The latter five minerals are the focus of this report. Zircon, rutile, geikielite, baddeleyite, and qandilite are present in concentrations  $\sim 0.01\%$  or less because only one geikielite grain and none of the other four minerals were encountered in the course of counting  $>28000$  points over 14 samples of dolomite. In spite of their small abundance, the minerals are easily identified by their distinctively bright appearance in back-scattered electron images. Zircon, rutile, geikielite, baddeleyite, and qandilite are not likely products of retrograde metamorphism for two reasons. First, the five minerals form euhedral crystals typically isolated in carbonate. Retrograde minerals are texturally different, replacing prograde minerals, e.g., brucite replaces periclase, serpentine replaces forsterite, chlorite replaces spinel, etc. (Ferry unpublished manuscript). Second, equilibria involving zircon, rutile, geiki-

elite, baddeleyite, forsterite, calcite, and dolomite record  $T-X_{CO_2}$  conditions consistent with those of the peak contact metamorphism independently determined by prograde mineral assemblages in carbonate and pelitic rocks from the Allt Guibhsachain area (presented below).

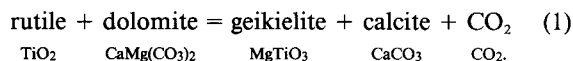
Qualitative analyses of zircon, rutile, and baddeleyite indicate that they are close to  $ZrSiO_4$ ,  $TiO_2$ , and  $ZrO_2$ , respectively. Geikielite is a  $(Mg,Fe,Mn)TiO_3$  solution with a quite variable  $Mg/(Mg + Fe + Mn)$  in the range 0.45–0.86 (Table 2). Qandilite, a rare Mg-Ti-rich spinel, has a composition in sample 3A almost the same as the type specimen from Iraq (Al-Hermezi 1985). Using Ti atoms per formula unit as a measure, qandilite in sample 3A has a mole fraction of the  $Mg_2TiO_4$  component  $\approx 0.6$ . Qandilite in sample 3B is significantly richer in the  $Fe_3O_4$  component. In both samples qandilite coexists with spinel *sensu stricto*, demonstrating the existence of a wide miscibility gap between  $MgAl_2O_4$ -rich and  $Mg_2TiO_4$ -rich spinels at the conditions of contact metamorphism.

### THREE NOVEL ISOGRADS

Because geikielite, baddeleyite, and qandilite tend to occur as isolated grains in carbonate and because of their very low concentrations, conventional considerations of textures and modal changes are useless in identifying the prograde reactions responsible for formation of the minerals. Nevertheless rutile, zircon, geikielite, baddeleyite, and qandilite display a regular spatial distribution in the Allt Guibhsachain area. Model prograde geikielite-, baddeleyite-, and qandilite-forming reactions were inferred from the distribution, and isograds were mapped on the basis of those reactions.

#### Geikielite isograd

At the lowest grades sampled in the Allt Guibhsachain area (locations 5, 6, 7A, Fig. 1) siliceous dolomites contain rutile, zircon, and dolomite but no geikielite, baddeleyite, or qandilite. Geikielite and calcite are present in and rutile + dolomite are absent from sample 7B and (with one exception) all others from higher-grade locations up to the contact between dolomite and granite at location 1. A model reaction that accounts for the prograde appearance of geikielite + calcite and disappearance of rutile + dolomite is



A geikielite isograd based on Reaction 1 can be mapped between locations 7A and 7B (Fig. 1). Because the exposure of siliceous dolomite is insufficient to locate the exact position of the isograd, it was drawn parallel to the strike of isograds in pelitic rocks in the area (Pattison and Harte 1991). Reactant and products occur together in only one sample (7D, Fig. 1). Natural geikielite contains significant amounts of Fe and Mn because of the strong partitioning of Fe and Mn into geikielite relative to other minerals in siliceous dolomites (Table 2). The composition of geikielite in individual samples and the stabili-

TABLE 2. Compositions of minerals in selected samples of metamorphosed siliceous dolomite

Sample	1A	2A	3A	3B	7A	7C	8A
<b>Matrix calcite</b>							
Ca	0.924	0.948	0.965	0.963	0.933	0.913	0.943
Mg	0.070	0.050	0.034	0.036	0.066	0.082	0.055
Fe	0.001	0.001	0.000	0.000	0.001	0.002	0.001
Mn	0.005	0.001	0.001	0.001	0.000	0.003	0.001
Oxide sum	56.06	56.28	55.64	55.66	56.02	55.86	56.08
<b>Inclusion calcite</b>							
Ca	0.862	0.855	0.860		0.909	0.905	
Mg	0.129	0.141	0.138		0.090	0.087	
Fe	0.003	0.002	0.000		0.001	0.004	
Mn	0.006	0.002	0.002		0.000	0.004	
Oxide sum	56.64	56.14	55.87		55.42	56.58	
T (°C)*	735	755	755		650	645	
<b>Dolomite</b>							
Ca	1.027	1.030	1.042	1.033	1.010	1.014	1.030
Mg	0.954	0.962	0.952	0.959	0.981	0.954	0.962
Fe	0.009	0.006	0.002	0.004	0.009	0.024	0.006
Mn	0.010	0.002	0.004	0.003	0.000	0.008	0.002
Oxide sum	52.15	52.35	52.50	52.39	52.13	51.96	52.25
<b>Forsterite</b>							
Mg	1.931	1.954	1.975	1.976	1.960	1.907	1.950
Fe	0.051	0.032	0.012	0.021	0.037	0.083	0.038
Mn	0.012	0.002	0.004	0.004	0.001	0.010	0.002
Ca	0.002	0.002	0.004	0.001	0.001	0.001	0.001
Si	1.001	1.003	1.001	0.996	0.998	0.997	1.004
Oxide sum	100.59	100.18	99.99	100.29	100.22	100.38	99.46
Fe/(Fe + Mg)	0.026	0.016	0.006	0.011	0.019	0.042	0.019
<b>Diopside</b>							
Ca					0.986	0.963	
Na					0.009	0.025	
Mg					0.969	0.915	
Fe					0.013	0.068	
Mn					0.000	0.009	
Ti					0.002	0.002	
Al					0.019	0.012	
Si					1.998	2.005	
Oxide sum					100.72	100.77	
Fe/(Fe + Mg)					0.013	0.070	
<b>Tremolite</b>							
K	0.006	0.007			0.007	0.029	0.005
Na	0.000	0.000			0.251	0.690	0.007
Ca	1.899	1.972			1.926	1.555	1.979
Na	0.069	0.019			0.074	0.445	0.021
Mg	4.813	4.769			4.786	4.696	4.897
Fe	0.124	0.062			0.056	0.211	0.042
Mn	0.015	0.009			0.005	0.016	0.002
Ti	0.007	0.010			0.022	0.015	0.008
<sup>6</sup> Al	0.072	0.151			0.134	0.151	0.036
<sup>4</sup> Al	0.027	0.141			0.372	0.636	0.014
Si	7.973	7.859			7.628	7.364	7.986
F	bd	bd			bd	bd	0.027
Oxide sum	98.56	97.48			97.88	97.70	97.87
Fe/(Fe + Mg)	0.025	0.013			0.012	0.043	0.009
<b>Spinel</b>							
Mg	0.935	0.946	0.985	0.972			0.957
Fe <sup>2+</sup>	0.067	0.055	0.025	0.033			0.045
Mn	0.009	0.003	0.003	0.002			0.001
Ca	0.002	0.001	0.004	0.001			0.001
Ti	0.013	0.005	0.017	0.007			0.003
Al	1.884	1.975	1.884	1.932			1.987
Fe <sup>3+</sup>	0.089	0.015	0.081	0.053			0.006
Oxide sum	99.95	100.01	99.50	100.39			99.55
<b>Mica</b>							
K	0.426	0.922					
Na	0.151	0.002					
Ba	0.406	0.021					
Mg	2.625	2.602					
Fe	0.096	0.042					
Mn	0.004	0.000					
Ti	0.088	0.075					

TABLE 2.—Continued

Sample	1A	2A	3A	3B	7A	7C	8A
<sup>63</sup> Al	0.175	0.249					
<sup>69</sup> Al	1.719	1.308					
Si	2.281	2.692					
F	0.005	bd					
Oxide sum	96.97	95.72					
Fe/(Fe + Mg)	0.035	0.016					
			<b>Geikielite</b>				
Mg	0.635	0.864				0.569	0.722
Fe	0.278	0.141				0.392	0.278
Mn	0.103	0.007				0.052	0.014
Ti	0.993	0.994				0.994	0.992
Oxide sum	100.18	100.38				99.46	100.15
Fe/(Fe + Mg)	0.304	0.140				0.408	0.278
			<b>Qandilite</b>				
Mg			1.215	0.965			
Fe <sup>2+</sup>			0.205	0.324			
Mn			0.159	0.131			
Ca			0.003	0.008			
Fe <sup>3+</sup>			0.742	1.055			
Al			0.093	0.092			
Cr			0.000	0.000			
Ti			0.583	0.426			
Oxide sum			97.09	95.7			

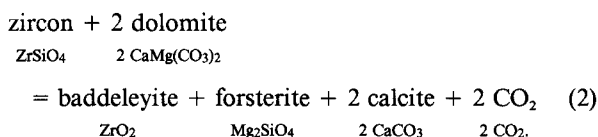
Note: Oxide sum refers to the sum of metal oxide weight percents with all Fe as FeO; bd = below detection limits. Sample numbers refer to Figure 1. Except for calcite, analyses are averages of 3–5 spot analyses of 3–5 grains in thin section. Calcite = cations per O atom (less CO<sub>2</sub>). Matrix calcite = average of 10–20 calcite grains in matrix; inclusion calcite = most magnesian analyzed calcite inclusion in forsterite. Dolomite = cations per 2 O atoms (less CO<sub>2</sub>). Forsterite = cations per 4 O atoms. Diopside = cations per 6 O atoms. Tremolite = cations per 23 O atoms (less H<sub>2</sub>O). Spinel and qandilite = cations per 3 total cations. Mica = cations per 11 O atoms (less H<sub>2</sub>O). Geikielite = cations per 3 O atoms. Fe in all but spinel and qandilite taken as Fe<sup>2+</sup>; Fe<sup>3+</sup>/Fe<sup>2+</sup> in spinel and qandilite adjusted to balance 8 negative charges.

\* Calcite + dolomite temperature (Anovitz and Essene 1987).

zation of reactants and products of Reaction 1 therefore depend sensitively on whole-rock Fe- and Mn-contents as well as *P*, *T*, and *X*<sub>CO<sub>2</sub></sub>.

**Baddeleyite isograd**

Zircon + dolomite occur in sample 7D and all others at lower grades; baddeleyite + forsterite + calcite are present in and zircon + dolomite are absent from sample 8A and all others at higher grades. A model reaction that accounts for the prograde appearance of baddeleyite + forsterite + calcite and disappearance of zircon + dolomite is

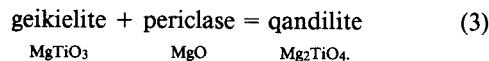


A baddeleyite isograd based on Reaction 2 can be mapped between locations 7D and 8A (Fig. 1). Like the geikielite isograd, the baddeleyite isograd was drawn parallel to the strike of isograds in pelitic rocks for lack of better constraints. The baddeleyite isograd in Figure 1 perfectly separates occurrences of reactants from occurrences of products of Reaction 2; reactants and products are present together in no sample.

**Qandilite isograd**

Geikielite occurs in sample 1A and all others at lower

grades within ~400 m of the contact; qandilite is present in and geikielite is absent from both samples collected from the dolomite xenolith at location 3. In principle, qandilite could form by reaction of geikielite with either dolomite or periclase. Siliceous dolomites from the Allt Guibhsachain area are uninformative as to which is the case because none contains either qandilite + dolomite or geikielite + periclase. Unpublished studies of siliceous dolomites in the Beinn an Dubhaich aureole, Scotland (Holness 1992), and the Silver Star aureole, Montana (Foote 1986), however, reveal coexisting geikielite + periclase in 22 samples and no occurrences of qandilite + dolomite. Consequently periclase forms in siliceous dolomites at grades lower than the qandilite isograd. A model reaction that accounts for the prograde appearance of qandilite and disappearance of geikielite + periclase is



A qandilite isograd based on Reaction 3 can be mapped between locations 1 and 3, and it was drawn parallel to the strike of isograds in pelitic rocks for lack of better constraints (Fig. 1). Reaction 3 only describes the formation of the Mg<sub>2</sub>TiO<sub>4</sub> component of qandilite; it does not account either for the significant Fe-content of the mineral (Table 2) or for the oxidation of Fe that probably occurs during the formation of the mineral.

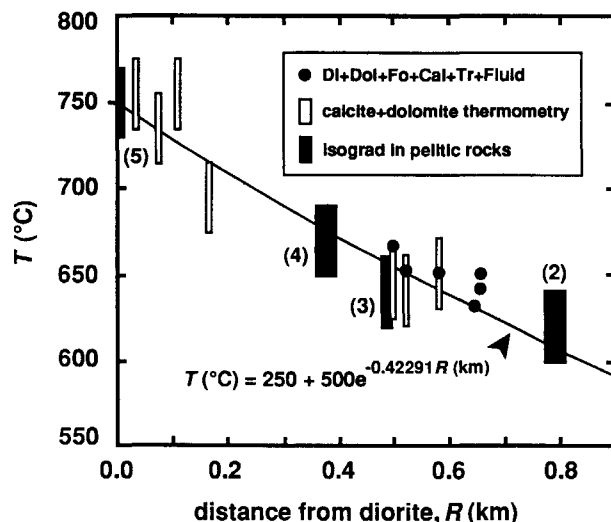


FIGURE 2. Temperature profile radial to the pluton in the Allt Guibhsachain area of the Ballachulish aureole. Distance,  $R$ , is measured from the outermost exposure of diorite rather than the outermost exposure of plutonic rock. Temperatures and distances for the pelitic isograds are from Pattison (1991); other results are from this study (see text). Isograds in pelitic rocks are based on the prograde appearance cordierite + potassium feldspar (2), andalusite + potassium feldspar (3), corundum + potassium feldspar (4), and silicate melt (5). Equation is for the curve and represents a least-squares fit to the data for pelitic isograds.

#### PHASE EQUILIBRIA AND PHYSICAL CONDITIONS AT THE ISOGRADS

##### Pressure and temperature during metamorphism in the Allt Guibhsachain area

Mineral equilibria in both pelitic rocks and siliceous dolomites from the Ballachulish aureole record a peak lithostatic pressure during contact metamorphism of  $3.0 \pm 0.5$  kbar (Pattison 1991; Masch and Heuss-Abichler 1991).

Positions of isograds in pelitic rocks in the northeast corner of the Ballachulish aureole and peak temperatures recorded by them are plotted in Figure 2 (from Table 16.4 of Pattison 1991). The size of each solid rectangle corresponds to Pattison's estimates of uncertainty in  $T$  and distance ( $R$ ). Thermal models of the aureole indicate that the diorite was the principal heat source for contact metamorphism (Buntebarth 1991). Following the precedent of Pattison (1991, 1992) and Masch and Heuss-Abichler (1991) values of  $R$  in Figure 2 therefore are measured radially from the outermost exposure of diorite. Temperatures for the pelitic isograds at  $R < 800$  m along with Buntebarth's best estimate for peak  $T$  at the contact ( $760 \pm 10$  °C) were fit by least-squares to an exponential function of  $R$  subject to the constraint that  $T = 250$  °C far from the intrusion (Buntebarth 1991):

$$T (\text{°C}) = 250 + 500e^{-0.42291R(\text{km})} \quad (4)$$

which corresponds to the curve in Figure 2.

Temperatures recorded by the most magnesian calcite

inclusion in forsterite (Table 2) in seven samples are shown as open rectangles in Figure 2. The size of each open rectangle corresponds to uncertainties of  $\pm 5$  m in  $R$  and  $\pm 20$  °C in  $T$  (representing an uncertainty of approximately  $\pm 0.5$  mol%  $\text{MgCO}_3$  in calcite composition). Calcite + dolomite temperatures are not reported for those forsterite-bearing dolomites in which either forsterite grains lack calcite inclusions, the calcite inclusions have exsolved dolomite, or the compositions of all analyzed calcite inclusions have been altered by communication between inclusions and the rock matrix via fractures. Inclusions with the maximum Mg-content were almost certainly in equilibrium with dolomite when they formed because forsterite developed in dolomite-bearing rocks either by a reaction between tremolite and dolomite or between diopside and dolomite (Masch and Heuss-Abichler 1991). Nevertheless, the temperatures recorded by calcite + dolomite thermometry formally are minimum estimates because the calcite may not have been included in forsterite and isolated from dolomite at peak metamorphic conditions. The average deviation of calcite + dolomite temperatures from the curve in Figure 2 is  $+1$  °C (range  $-21$  to  $+28$  °C). Although the inclusions may not have formed precisely at the peak of metamorphism, they evidently record peak temperature within error of measurement. With one exception, calcite + dolomite temperatures reported for the Allt Guibhsachain area by Masch and Heuss-Abichler (1991) fall below the curve (their results not plotted in Fig. 2). Although they carefully sought the most Mg-rich calcite in each sample, their slightly lower temperatures probably result from analyzing matrix grains whose compositions were partially reset during cooling by dolomite exsolution.

Temperatures recorded by equilibrium among diopside, dolomite, forsterite, calcite, tremolite, and fluid at  $P_{\text{CO}_2} + P_{\text{CO}_2} = P = 3.0$  kbar were calculated for six samples of siliceous dolomite with the use of Berman's (1988) data base (updated August 1990); the Kerrick and Jacobs (1981) equation of state for  $\text{CO}_2$ - $\text{H}_2\text{O}$  fluid; and Skippen's (1974) model for calcite solutions coexisting with dolomite; measured compositions of diopside, forsterite, and tremolite; simple ideal ionic mixing models for diopside and forsterite; and the expression for tremolite activity from Holland and Powell (1990) assuming random mixing of cations over the M1, M2, and M3 sites. Results appear as solid circles in Figure 2. The size of circles has no meaning because uncertainties in the calculated temperatures are unknown. The average deviation in temperature of the six-phase equilibrium from the curve is  $+10$  °C (range  $+1$  to  $+22$  °C).

The good agreement between temperatures recorded by the three independent mineral equilibria and the model curve in Figure 2 is justification for using them to constrain temperature and fluid composition during formation of geikielite, baddeleyite, and qandilite.

##### Baddeleyite isograd

Thermodynamic analysis of the baddeleyite isograd is

the most straightforward of the three because zircon and baddeleyite are not complicated by significant solid solution. Figure 3 illustrates phase equilibria involving calcite, dolomite, diopside, tremolite, forsterite, zircon, and baddeleyite calculated from the data base of Berman (1988; updated August 1990, by personal communication) with unit activities for all mineral components except calcite whose composition is adjusted for coexistence with dolomite. Solid circles illustrate the  $T$ - $X_{\text{CO}_2}$  conditions of equilibration of the six occurrences of the diopside + dolomite + forsterite + calcite + tremolite + fluid equilibrium with reduced activity of the tremolite component in amphibole labeled for each point. The compositions of dolomite, diopside, forsterite, and calcite in the samples deviate only slightly from those of ideal compounds in the system  $\text{CaO-MgO-SiO}_2\text{-CO}_2\text{-H}_2\text{O}$ . The six-phase assemblage is stabilized in the aureole over a  $\sim 30^\circ\text{C}$  interval largely by a reduction in tremolite activity. The  $T$ - $X_{\text{CO}_2}$  conditions recorded by the samples therefore lie close to the diopside + dolomite + forsterite + calcite equilibrium curve at temperatures between the diopside + dolomite + forsterite + calcite + tremolite invariant point for unit activity of tremolite and  $X_{\text{CO}_2} = 1$  (Fig. 3).

The baddeleyite isograd is mapped between locations 7D and 8A (Fig. 1). Peak temperatures at the locations, based on the model profile in Figure 2, are  $660$  and  $710^\circ\text{C}$ , respectively. If fluid composition at the baddeleyite isograd was the same as at the peak of metamorphism at locations 7A–7C,  $X_{\text{CO}_2}$  was  $0.76$ – $0.95$ . The inferred  $T$ - $X_{\text{CO}_2}$  conditions for the isograd therefore are those of the shaded rectangle in Figure 3. The  $T$ - $X_{\text{CO}_2}$  curve for baddeleyite-forming Reaction 2, independently calculated from Berman's data base, passes through the middle of the rectangle.

### Geikielite isograd

The geikielite isograd is mapped between locations 7A and 7B (Fig. 1). The minimum peak temperature estimated for location 7A is that of the model temperature profile in Figure 2,  $640^\circ\text{C}$ . The maximum peak temperature estimated for location 7B is that recorded by the diopside + dolomite + forsterite + calcite + tremolite + fluid equilibrium,  $655^\circ\text{C}$ . The  $X_{\text{CO}_2}$  of fluid recorded by the six-phase equilibrium at locations 7A and 7B is  $0.76$  and  $0.80$ , respectively. The inferred  $T$ - $X_{\text{CO}_2}$  conditions for the geikielite isograd therefore are those of the shaded rectangle in Figure 4.

The  $T$ - $X_{\text{CO}_2}$  curve for geikielite-forming Reaction 1 with unit activity for the geikielite component, calculated from Berman's data base, is significantly removed from the shaded rectangle in Figure 4. Analysis of phase equilibria for Reaction 1, however, must consider the deviation in composition of natural geikielite from  $\text{MgTiO}_3$ , as well as  $T$  and  $X_{\text{CO}_2}$ . Dashed curves in Figure 4 illustrate how the  $T$ - $X_{\text{CO}_2}$  conditions for Reaction 1 are displaced by reduced geikielite activities in the range  $0.6$ – $1.0$ . Circles in Figure 4 represent the  $T$ - $X_{\text{CO}_2}$  conditions of the six oc-

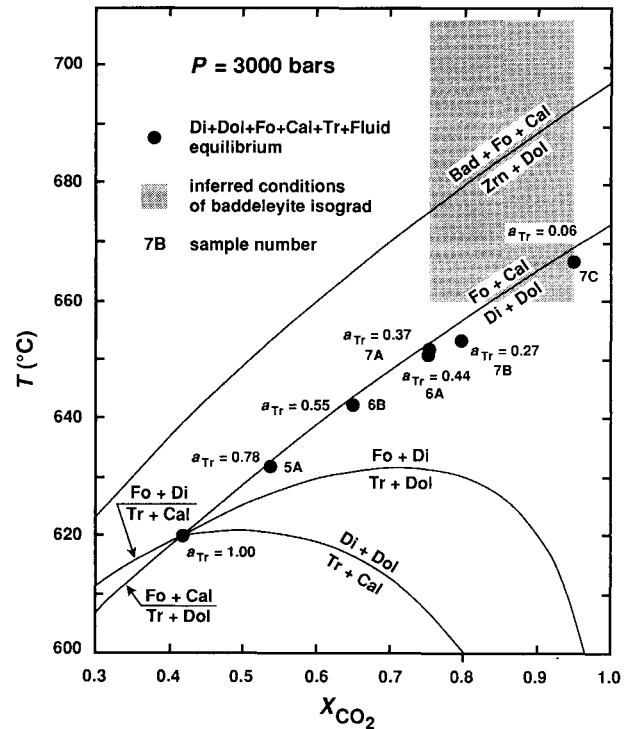
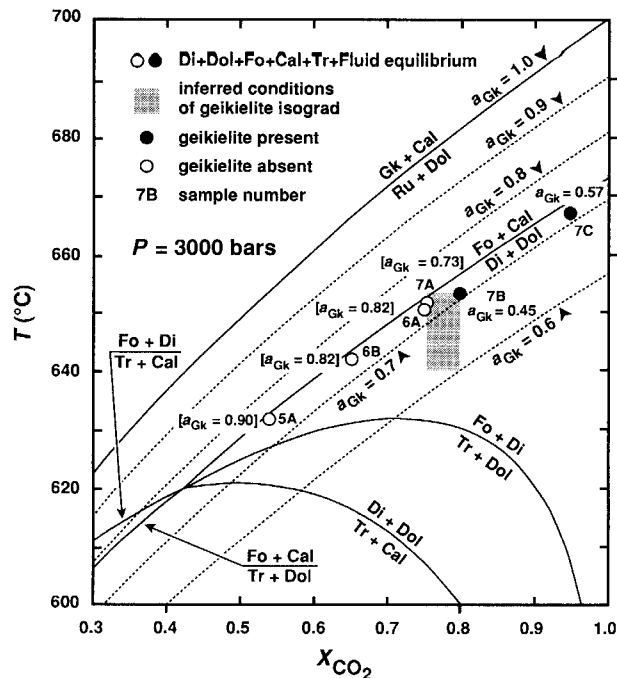


FIGURE 3.  $T$ - $X_{\text{CO}_2}$  diagram depicting phase equilibria among diopside (Di), dolomite (Dol), forsterite (Fo), calcite (Cal), tremolite (Tr), zircon (Zrn), baddeleyite (Bad), and  $\text{CO}_2$ - $\text{H}_2\text{O}$  fluid at 3 kbar calculated from Berman's (1988) data base, updated August 1990. All minerals except Cal and Tr are assumed to be pure substances. Cal compositions were adjusted for equilibrium with Dol. Solid circles represent  $T$ - $X_{\text{CO}_2}$  conditions estimated for six occurrences of the assemblage Di + Dol + Fo + Cal + Tr with reduced Tr activity ( $a_{\text{Tr}}$ ) as indicated; unit Tr activity assumed along calculated curves. Conditions of the baddeleyite isograd predicted by the Zrn + Dol + Bad + Fo + Cal equilibrium are consistent with independently inferred conditions based on other mineral-fluid equilibria (shaded rectangle).

currences of the diopside + dolomite + forsterite + calcite + tremolite + fluid equilibrium in the aureole (same as circles in Fig. 3). The number by each solid circle is the activity of geikielite in the sample (estimated from measured mineral compositions assuming ideal mixing). The number by each open circle is the activity of  $\text{MgTiO}_3$  in a fictive geikielite in Fe-Mg and Mn-Mg exchange equilibrium with forsterite that would have developed should the  $T$ - $X_{\text{CO}_2}$  conditions have been appropriate for formation of the oxide. The composition of the fictive geikielite (Gk) was calculated from measured forsterite (Fo) composition in each sample taking  $(\text{Fe}/\text{Mg})_{\text{Gk}}/(\text{Fe}/\text{Mg})_{\text{Fo}} = 19.2$  and  $(\text{Mn}/\text{Mg})_{\text{Gk}}/(\text{Mn}/\text{Mg})_{\text{Fo}} = 22.2$  (the average of  $K_D$  values for seven analyzed geikielite-forsterite pairs from the area).

Figure 4 quantitatively explains the occurrence and absence of geikielite in the Allt Guibhsachain area in terms of  $T$ ,  $X_{\text{CO}_2}$ , and mineral composition. Geikielite devel-



**FIGURE 4.**  $T$ - $X_{\text{CO}_2}$  diagram depicting phase equilibria among diopside (Di), dolomite (Dol), forsterite (Fo), calcite (Cal), tremolite (Tr), rutile (Ru), geikielite (Gk), and  $\text{CO}_2$ - $\text{H}_2\text{O}$  fluid at 3 kbar calculated from Berman's (1988) data base, updated August 1990. All minerals except Cal and Gk are assumed to be pure substances. Cal compositions were adjusted for equilibrium with Dol. Dashed curves show how the Ru + Dol + Gk + Cal equilibrium is displaced by reduced activity of  $\text{MgTiO}_3$  ( $a_{\text{Gk}}$ ). Circles represent  $T$ - $X_{\text{CO}_2}$  conditions estimated for six occurrences of the assemblage Di + Dol + Fo + Cal + Tr (from Fig. 3). Values of  $a_{\text{Gk}}$  next to solid circles are based on measured Gk compositions in the sample. Values of  $a_{\text{Gk}}$  in brackets next to open circles are fictive values estimated from Fe-Mg and Mn-Mg exchange equilibria between Fo and Gk and the composition of Fo in the sample. Gk develops in rocks with Ru + Dol by Reaction 1 at  $T$ - $X_{\text{CO}_2}$  conditions above the dashed  $a_{\text{Gk}}$  contour corresponding to Gk composition in that rock. Gk fails to form in rocks with Ru + Dol by Reaction 1 at  $T$ - $X_{\text{CO}_2}$  conditions on or below the dashed  $a_{\text{Gk}}$  contour corresponding to composition of fictive Gk that would occur in the sample (see text).

oped in those samples (solid circles) metamorphosed at  $T$ - $X_{\text{CO}_2}$  conditions above the dashed  $a_{\text{Gk}}$  contour corresponding to geikielite composition in the sample. Although not plotted on Figure 4 because peak values of  $X_{\text{CO}_2}$  are unconstrained, geikielite-bearing rocks between locations 8A and 1A must plot likewise because estimated peak  $T$  is higher than  $T$  for  $a_{\text{Gk}} = X_{\text{CO}_2} = 1$ . The occurrence of rutile + dolomite + geikielite + calcite in sample 7D could not be evaluated because geikielite grains in the rock are too small for analysis. Geikielite failed to develop in those samples (open circles) metamorphosed

on or below the dashed  $a_{\text{Gk}}$  contour corresponding to the composition of fictive geikielite that would have developed had  $T$ - $X_{\text{CO}_2}$  conditions been appropriate for formation of the mineral by Reaction 1. Development of geikielite by Reaction 1 near the isograd evidently was limited to relatively Fe- and Mn-rich rocks ( $a_{\text{Gk}}$  less than  $\sim 0.7$ ); at  $T > 700$  °C, however, formation of geikielite in rocks with rutile + dolomite was independent of whole-rock Fe- and Mn-contents. The excellent agreement between the model for geikielite-formation in Figure 4 and the observed presence or absence of geikielite in siliceous dolomites from the Allt Guibhsachain area suggests that the accuracy of thermodynamic values for rutile and geikielite in Berman's data base is sufficient for meaningful estimates of  $T$  and  $X_{\text{CO}_2}$  from equilibria involving the two minerals.

#### Qandilite isograd

The qandilite isograd is mapped between locations 1 and 3 (Fig. 1). Because sample 1A did not contain periclase and probably did not contain dolomite at the peak of metamorphism, the physical conditions of the qandilite isograd are bracketed by those at location 3 and those of the next lower grade sample from 1A that contains peak dolomite, 2A. The minimum peak temperature estimated for location 2 is that of the model temperature profile in Figure 2, 725 °C. The maximum peak temperature estimated for location 3 is that recorded by the composition of calcite inclusions in forsterite from sample 3A, 755 °C. Qandilite formed in the stability field of periclase which lies at  $X_{\text{CO}_2} < 0.08$  for  $T < 755$  °C. The inferred  $T$ - $X_{\text{CO}_2}$  conditions for the qandilite isograd therefore are  $T = 725$ – $755$  °C and  $X_{\text{CO}_2} < 0.08$ . Because there are no data for  $\text{Mg}_2\text{TiO}_4$  in any of the current thermodynamic data bases, the indirectly inferred conditions for its formation could not be compared to conditions directly computed from equilibria involving qandilite and other minerals in the siliceous dolomites.

## DISCUSSION

### Novel and conventional isograds in siliceous dolomites

Isograds based on the formation of geikielite, baddeleyite, and qandilite in siliceous dolomites supplement conventional isograds. All three minerals developed in forsterite-bearing rocks and therefore their isograds lie at grades higher than the forsterite isograd. The baddeleyite isograd occurs in the vicinity of the diopside-out isograd (which in Si-poor dolomites corresponds to completion of the diopside + dolomite + forsterite + calcite reaction in Figs. 3 and 4). Calculated phase equilibria in Figure 3 and field occurrences in Figure 1, however, more narrowly bracket the baddeleyite isograd between the diopside-out and periclase isograds. The qandilite isograd occurs in the vicinity of the periclase isograd. Coexisting geikielite + periclase, however, are commonly observed in the

Beinn an Dubhaich and Silver Star aureoles. The qandilite isograd in the Allt Guibhsachain area therefore probably lies at grades higher than the periclase isograd (Fig. 1) but at grades lower than the monticellite isograd in Si-poor dolomites. The geikielite, baddeleyite, and qandilite isograds offer increased resolution of metamorphic grade at high but not the highest temperatures of crustal metamorphism.

#### Equilibria involving trace minerals in metamorphosed siliceous dolomites

The trace minerals rutile, zircon, geikielite, baddeleyite, and qandilite compose <0.01% of siliceous dolomites from the Allt Guibhsachain area. Nevertheless, they evidently reacted both with each other and with more abundant coexisting carbonate and silicate minerals in a regular fashion producing a systematic pattern of isograds. Furthermore, physical conditions of metamorphism predicted independently from carbonate-silicate-fluid equilibria are the same within error as those predicted directly from equilibria involving rutile, geikielite, zircon, baddeleyite, calcite, dolomite, forsterite, and fluid. The agreement leads to two conclusions. First, in spite of their small abundance and refractory character, the trace minerals appear to have been in local equilibrium during metamorphism both with each other and with the principal minerals in each specimen. Second, because the trace minerals appear to record equilibrium, they have the potential to provide information about the  $P-T-X_{CO_2}$  conditions of metamorphism. Their usefulness may be general and widespread. Trace amounts of combinations of rutile, zircon, geikielite, and baddeleyite are common in forsterite-bearing siliceous dolomites from the Ballachulish, Beinn an Dubhaich, and Silver Star aureoles, and the minerals may have been overlooked at other locations. Silicate minerals in many siliceous dolomites are completely altered to retrograde minerals such as serpentine and chlorite. Occurrences of the more refractory minerals rutile, zircon, geikielite, and baddeleyite, if preserved in such rocks, may in fact represent the only usable mineralogical record of physical conditions at the peak of contact metamorphism.

#### Dating a prograde mineral reaction

Measurement of the radiometric age of baddeleyite in siliceous dolomites from the Allt Guibhsachain area (and other aureoles) would determine the age of Reaction 2 and of prograde contact metamorphism itself, provided the closure  $T$  for baddeleyite is greater than  $\sim 700^\circ\text{C}$ . Practically, however, dating of baddeleyite could be limited by its very small abundance in the dolomites.

#### ACKNOWLEDGMENTS

Ben Harte and Dave Pattison clarified many aspects of contact metamorphism in the Ballachulish aureole both in and out of the field. Don

Lindsay provided the reference to the type specimen of qandilite, and Steve Guggenheim gave advice on the occurrence and chemistry of kinoshitalite. Thoughtful reviews by Martha Gerdes and Dave Pattison are gratefully appreciated. Research support by the National Science Foundation, Division of Earth Sciences, grant EAR-9404578.

#### REFERENCES CITED

- Al-Hermezi, H.M. (1985) Qandilite, a new spinel end-member,  $Mg_2TiO_4$ , from the Qala-Dizeh region, NE Iraq. *Mineralogical Magazine*, 49, 739–744.
- Anovitz, L.M., and Essene, E.J. (1987) Phase equilibria in the system  $CaCO_3$ - $MgCO_3$ - $FeCO_3$ . *Journal of Petrology*, 19, 389–414.
- Armstrong, J.T. (1988) Quantitative analysis of silicate and oxide minerals: Comparison of Monte Carlo, ZAF and phi-rho-z procedures. In D.E. Newbury, Ed., *Microbeam analysis*, p. 239–246. San Francisco Press, California.
- Berman, R.G. (1988) Internally-consistent thermodynamic data for minerals in the system  $Na_2O$ - $K_2O$ - $CaO$ - $MgO$ - $FeO$ - $Fe_2O_3$ - $Al_2O_3$ - $SiO_2$ - $TiO_2$ - $H_2O$ - $CO_2$ . *Journal of Petrology*, 29, 445–522.
- Bowen, N.L. (1940) Progressive metamorphism of siliceous limestone and dolomite. *Journal of Geology*, 48, 225–274.
- Buntbarth, G. (1991) Thermal models of cooling. In G. Voll, J. Töpel, D.R.M. Pattison, and F. Seifert, Eds., *Equilibrium and kinetics in contact metamorphism: The Ballachulish igneous complex and its aureole*, p. 379–402. Springer-Verlag, Berlin.
- Footo, M.W. (1986) Contact metamorphism and skarn development of the precious and base metal deposits at Silver Star, Madison County, Montana. Ph.D. thesis, University of Wyoming, Laramie.
- Heuss-Abbichler, S., and Masch, L. (1991) Microtextures and reaction mechanisms in carbonate rocks: A comparison between the thermo-aureoles of Ballachulish and Monzoni (Italy). In G. Voll, J. Töpel, D.R.M. Pattison, and F. Seifert, Eds., *Equilibrium and kinetics in contact metamorphism: The Ballachulish igneous complex and its aureole*, p. 229–249. Springer-Verlag, Berlin.
- Holland, T.J.B., and Powell, R. (1990) An enlarged and updated internally consistent thermodynamic dataset with uncertainties and correlations: The system  $K_2O$ - $Na_2O$ - $CaO$ - $MgO$ - $MnO$ - $FeO$ - $Fe_2O_3$ - $Al_2O_3$ - $SiO_2$ - $TiO_2$ - $C$ - $H_2O$ - $O_2$ . *Journal of Metamorphic Geology*, 8, 89–124.
- Holness, M.B. (1992) Metamorphism and fluid infiltration of the calc-silicate aureole of the Beinn an Dubhaich granite, Skye. *Journal of Petrology*, 33, 1261–1293.
- Kerrick, D.M., and Jacobs, G.K. (1981) A modified Redlich-Kwong equation for  $H_2O$ ,  $CO_2$ , and  $H_2O$ - $CO_2$  mixtures at elevated pressures and temperatures. *American Journal of Science*, 281, 735–767.
- Kretz, R. (1983) Symbols for rock-forming minerals. *American Mineralogist*, 68, 277–279.
- Masch, L., and Heuss-Abbichler, S. (1991) Decarbonation reactions in siliceous dolomites and impure limestones. In G. Voll, J. Töpel, D.R.M. Pattison, and F. Seifert, Eds., *Equilibrium and kinetics in contact metamorphism: The Ballachulish igneous complex and its aureole*, p. 211–227. Springer-Verlag, Berlin.
- Pattison, D.R.M. (1991)  $P$ - $T$ - $a(H_2O)$  conditions in the aureole. In G. Voll, J. Töpel, D.R.M. Pattison, and F. Seifert, Eds., *Equilibrium and kinetics in contact metamorphism: The Ballachulish igneous complex and its aureole*, p. 327–350. Springer-Verlag, Berlin.
- (1992) Stability of andalusite and sillimanite and the  $Al_2SiO_5$  triple point: Constraints from the Ballachulish aureole, Scotland. *Journal of Geology*, 100, 423–446.
- Pattison, D.R.M., and Harte, B. (1991) Petrography and mineral chemistry of pelites. In G. Voll, J. Töpel, D.R.M. Pattison, and F. Seifert, Eds., *Equilibrium and kinetics in contact metamorphism: The Ballachulish igneous complex and its aureole*, p. 135–179. Springer-Verlag, Berlin.
- Skippen, G.B. (1974) An experimental model for low pressure metamorphism of siliceous dolomitic marble. *American Journal of Science*, 274, 487–509.

Tilley, C.E. (1948) Earlier stages in the metamorphism of siliceous dolomites. *Mineralogical Magazine*, 28, 272-276.

Voll, G., Töpel, J., Pattison, D.R.M., and Seifert, F., Eds. (1991) Equilibrium and kinetics in contact metamorphism: The Ballachulish igneous complex and its aureole, 484 p. Springer-Verlag, Berlin.

Weiss, S. (1986) Petrogenese des intrusivkomplexes von Ballachulish,

Westschottland: Kristallisationsverlauf in einem zonierten Kaledonischen pluton. Ph.D. thesis, Ludwig-Maximilians-Universität, Munich.

MANUSCRIPT RECEIVED JUNE 16, 1995

MANUSCRIPT ACCEPTED NOVEMBER 16, 1995